Carbon Trends 5 (2021) 100126

Contents lists available at ScienceDirect

Carbon Trends

journal homepage: www.elsevier.com/locate/cartre

Improvements in the thermomechanical and electrical behavior of hybrid carbon-epoxy nanocomposites

J. López-Barroso [a,b], A.L. Martínez-Hernández [b], J.L. Rivera-Armenta [a], A. Almendárez-Camarillo [c], P.E. García-Casillas [d], C.G. Flores-Hernández [b], C. Velasco-Santos [b,*]

[a] División de Estudios de Posgrado e Investigación, Centro de Investigación en Petroquímica, Tecnológico Nacional de México Campus Ciudad Madero, Altamira, Tamaulipas 89600, Mexico
[b] División de Estudios de Posgrado e Investigación, Tecnológico Nacional de México Campus Querétaro, Santiago de Querétaro 76000, Mexico
[c] Departamento de ingeniería Química, Tecnológico Nacional de México Campus Celaya, Celaya, Guanajuato 38010, Mexico
[d] Universidad Autónoma de Ciudad Juárez Ciudad Juárez, Chihuahua 32310, Mexico

ARTICLE INFO

Article history:
Received 23 August 2021
Revised 26 October 2021
Accepted 27 October 2021

Keywords:
Hybrid composites
Carbon nanotubes
Graphene
Thermomechanical response
Raman mapping

ABSTRACT

In this work, polymeric composites of epoxy matrix reinforced with 1D and 2D nanocarbon allotropes are reported. Hybrid 3D nanostructures formed from 1D multi-walled carbon nanotubes and 2D graphene derivatives improve the electrical and thermomechanical response of the synthesized nanocomposites. Additionally, oxygenated moieties in the surface of the sp^2 carbon allotropes positively influences the dispersion of nanomaterials in the matrix and promote better interfaces among the polymeric matrix and reinforcements. Raman spectroscopy detects the different interactions of polymeric chains with carbon nanomaterials in different loads. Furthermore, Raman mapping shows the carbon dispersion regions and the influence on the final mechanical properties of the materials. The viscoelastic response evaluated by Dynamical Mechanical Analysis shows improvements of up to 138% in the storage modulus of nanocomposites with oxidized nanostructures in comparison to neat epoxy. 3D nanostructures changed the insulating nature of epoxy when the carbon nanomaterials formed the interconnected network. Some nanocomposites show an abrupt change from the insulator epoxy resin toward a semiconductor response, mainly in hybrids reinforced with pristine multi-walled carbon nanotubes and reduced graphene oxide. The TEM images of the nanocomposites showed interconnections between the 1D-2D hybrid carbon nanomaterials, which suggest a synergetic effect.

1. Introduction

In recent years, the study of sp^2 carbon allotropes has increased exponentially because of their outstanding and intrinsic properties. The carbon nanomaterials possess different nanostructure dimensions due to their different morphologies. Thus, there are four groups of carbon allotropes based on the sp^2 electronic configuration: fullerenes, nanotubes, graphene, and graphite, as zero (0D), one (1D), two (2D), and three (3D constructed by the nanostructures with fewer dimensions) dimensional. Consequently, like their predecessors (the carbon fiber reinforced composites), polymeric nanocomposites reinforced with carbon nanomaterials have become an essential piece in the field of materials, seeking to achieve high performance and multifunctional properties [1]. Therefore, different approaches to improve the physical properties have been developed involving the incorporation of one nanostructure into a polymeric matrix [2–7]. Nevertheless, the use of high amounts of these materials negatively affects the final mechanical properties. Thus, recent research has focused on obtaining better properties in nanocomposites with low nanostructure content. For instance, 3D nanostructures built from two or more nanomaterials have provided a new generation of multifunctional nanocomposites [7–12].

Graphene is considered the base of all graphitic materials [13–15]. The properties of graphene-derived nanomaterials are stunning. Unfortunately, π-π effects and the high Van der Waals forces of the materials (a result of its electronic configuration) restrict the complete transfer of its mechanical properties in nanocomposites when they are used as reinforcements [16,17]. In other

* Corresponding author.
E-mail address: cylaura@gmail.com (C. Velasco-Santos).

https://doi.org/10.1016/j.cartre.2021.100126

words, the carbon agglomeration issues in polymeric nanocomposites have not been resolved yet.

Different methods have been applied to disperse carbon nanoreinforcements in polymeric matrices, such as magnetic stirring, three-roll mill, or ultrasonic waves. The latter has shown good results [18]. Furthermore, complementary treatments such as chemical functionalization improve the dispersion through the affinity created among the functional groups and the matrix [5]. Hence, graphene-based materials acquired better interphase because of functional groups produced on their synthesis or functionalization [19,20]. The graphene oxide (O2D) obtained from the chemical route exhibits plenty of oxygen-containing functional groups over its surface [19]. Cote et al. [21] mentioned that the O2D has many sites with both hydrophilic (oxygen functional groups) and hydrophobic (aromatic regions) nature acting as adhesion points to the polymeric matrix. O2D acts as a surfactant to disperse the graphite, and the carbon nanotubes (CNT) were useful for disentangling them and co-assembling a hybrid 3D nanostructure. This hybrid offers the advantage of two kinds of nanostructures with outstanding results.

Nowadays, the study of 3D hybrid nanostructures is focused on transferring their outstanding properties to polymeric matrices for high-performance nanocomposites. There are reports of improved mechanical properties like hardness [22], tensile [16,23,24], and flexural [22]. Some reports have also focused on the electrical and thermal performance [16,23,24]. Moreover, the viscoelastic response of hybrid-reinforced polymeric composites has been reported [17,25,26]. Im and Kim [26] synthesized composites using O2D and multi-walled carbon nanotubes (M1D). They obtained higher values for both the storage modulus (E') and the glass transition temperature (T_g) of the epoxy. In that research, they highlighted the importance of oxygen-containing functional groups in improving the carbon reinforcements and matrix affinity. Besides, they observed improvements in thermal conductivity. However, it required the addition of a large amount of carbon nanomaterials (approximately 36 wt% and 50 wt% of blends of O2D and M1D for the thermal and mechanical response, respectively).

Araby et al. [25] demonstrated the establishment of conductive 3D networks. In this work, the 1D nanostructures (M1D) act as nanowires that transport electrons and stress to 2D nanostructures (graphene nanoplatelets, GNPT). Hence, the 1D-2D interconnected nanostructures work as a conductive path. Also, there are improvements in the hybrid reinforcement dispersion in the elastomeric matrix. The better dispersion reflects enhancements in the resistance to dynamic deformation due to the confinement of polymeric chains by the network M1D-GNPT.

This research reports the viscoelastic and electrical response of 1D & 2D carbon-reinforced nanocomposites. The Dynamical Mechanical Analysis (DMA) exhibits the influence of blends with functionalized and non-functionalized nanomaterials over the epoxy matrix. The thermomechanical results of 1D-2D reinforced nanocomposites suggest the appearance of 3D nanostructures. Electrical measurements show the synergetic effect obtained from the bridging between 1D & 2D geometries of nanomaterials. This effect impacts the electrical behavior of composites synthesized with a low carbon content.

2. Materials and methods

SUNNANO supplied the M1D. The M1D size ranges for the outer diameter and length are 10–30 nm and 1–10 µm, respectively. The graphite powder (GRA) was purchased from Electron Microscopy Science. The GRA is spectra-grade with an ash content < 2 ppm.

Sigma-Aldrich supplied most of the reagents used in the chemical functionalization of the 1D nanomaterials and the obtention of the 2D nanomaterials. The reagents were potassium permanganate ($KMnO_4$, 99%) and nitric (HNO_3, 70%), sulfuric (H_2SO_4, 98%), and hydrochloric (HCl, 37%) acid. No reagent from the list above was modified for use. Additionally, Baker supplied the hydrogen peroxide (H_2O_2, 30%) and ascorbic acid (LAA, this reagent was used in an aqueous solution at 20 mM).

For the epoxy matrix, the reagents used were 4,4′-isopropylidenediphenol diglycidyl ether (DGEBA, molecular weight 340.41 g mol^{-1} from the datasheet) and 1,2-diaminoethane (EDA, $>$ 99.5%, molecular weight 60.1 g mol^{-1} from the datasheet). According to the manufacturer, the stoichiometric EDA/DGEBA ratio is 8.8 w/w.

2.1. 2D materials synthesis

The O2D and reduced graphene oxide (RG2D) were synthesized by following the steps reported in [27]. Briefly, the graphite oxide (GRAOX) resulted from the oxidation of the GRA in a mixture of sulfuric acid (H_2SO_4, 98%) and potassium permanganate ($KMnO_4$, 99%) under magnetic stirring at 35 °C for 3 h.

For the O2D, 100 mg of GRAOX and 10 ml of water (distilled) were put in an ultrasound bath (Autoscience model 10200B) at a frequency of 40 kHz for 3 h at room temperature. The reduction reaction was made by adding the LAA with 1 mg ml^{-1} to the O2D solution under magnetic stirring for 20 min at 95 °C [28]. GRAOX, O2D, and RG2D were dried for 12 h after their synthesis at 65 °C under an air atmosphere (oven, Felisa FE-291 AD).

2.2. Functionalization of 1D reinforcements

The functionalization used for the 1D carbon nanomaterials involves two principal steps [27]. The first consisted of immersing the M1D in a blend of H_2SO_4 and HNO_3 (3:1 molar), and then the mixture was ultrasonicated for 30 min (Autoscience 10200B) at 40 kHz. The second step was to irradiate the acid sonicated M1D with microwaves (MW) immersed in H_2O_2. The exposure time was alternating between 1 min on and 1 min off and repeating this four times. After the oxidation, the multi-walled carbon nanotubes (O-M1D) were dried and stored for later use. An in-depth description of the 1D functionalization, 2D synthesis, and the resulting materials is provided in a previous report [27].

2.3. Synthesis of nanocomposites

The DGEBA and EDA reagents (10:1) were the matrix and hardener, respectively, for the nanocomposites. The nanomaterials were added in selected quantities to the epoxy to form two experiment matrices, as shown in Table 1. The mentioned quantities also were selected to avoid agglomerations, as other works mentioned [29–31]. Based on our previous work [27], two methods to transfer the resin to the mold with a geometry according to the norm ASTM D4065 (35 mm × 10 mm × 3.2 mm) were compared. The first method used for the multidimension nanocomposites (DI) consisted of pouring all the mixture (epoxy and 1D-2D reinforcement) in one-step followed by curing at 46 °C in an oven for 1 h (Fig. 1a).

For the second method (multilayer nanocomposites (LA), Fig. 1b), the polymer matrix and a calculated amount of nanoreinforcement were stacked four times. In other words, 6 g of resin with 1D or 2D nanomaterials built one layer according to the experimental matrix (see Table 1). After the nanomaterials were added to the resin, the mixture was put in an ultrasonic bath (Autoscience 10200B) for 1 h at 40 kHz. The blend was then poured into the mold and cured for 1 h at 46 °C. Subsequently, another layer was added over the cured material. This procedure was repeated four times, pouring one layer of 2D reinforcement followed by a layer of 1D reinforcement.

Table 1
Set of names used for the multidimension (DI) and multilayer (LA) nanocomposites* depending on the percentage and the kind of nanoreinforcements added.

Neat epoxy					
M1D	M1D	M1D-O2D	M1D-RG2D	O-M1D-O2D	O-M1D-RG2D
0.1 wt%.	0.5 wt%.	0.1–0.1 wt%	0.1–0.1 wt%	0.1–0.1 wt%	0.1–0.1 wt%
O-M1D	O-M1D	M1D- O2D	M1D- RG2D	O-M1D- O2D	O-M1D- RG2D
0.1 wt%.	0.5 wt%.	0.1–0.5 wt%	0.1–0.5 wt%	0.1–0.5 wt%	0.1–0.5 wt%
O2D	O2D	M1D- O2D	M1D- RG2D	O-M1D-O2D	O-M1D-RG2D
0.1 wt%.	0.5 wt%.	0.5–0.1 wt%	0.5–0.1 wt%	0.5–0.1 wt%	0.5–0.1 wt%
RG2D	RG2D	M1D- O2D	M1D- RG2D	O-M1D-O2D	O-M1D-RG2D
0.1 wt%	0.5 wt%	0.5–0.5 wt%	0.5–0.5 wt%	0.5–0.5 wt%	0.5–0.5 wt%

*In the discussion, the materials indicated as DI refers to multidimension nanocomposites, and LA matches to the multilayer nanocomposites. Both nomenclatures are related to the methodology of synthesis.

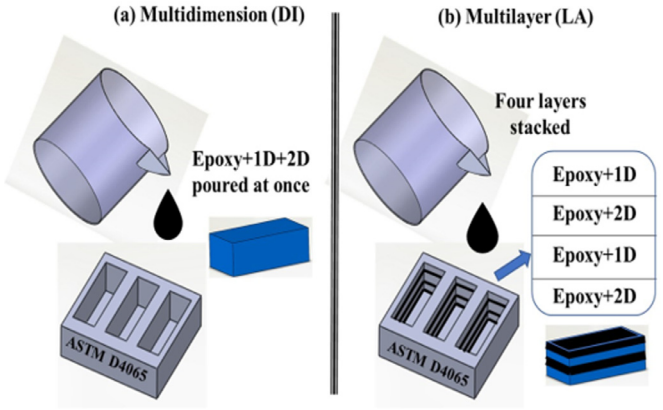

Fig. 1. Schematic diagram of the synthesis of (a) DI and (b) LA nanocomposites.

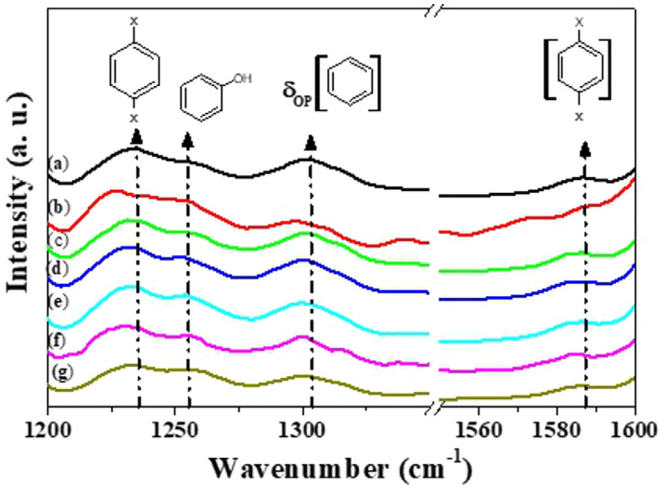

Fig. 2. Raman spectrum of DI nanocomposites (a) Neat epoxy DI; (b) M1D 0.1 wt% DI; (c) O-M1D 0.1 wt% DI; (d) O2D 0.1 wt% DI; (e) RG2D 0.1 wt% DI; (f) M1D-RG2D 0.1–0.1 wt% DI; (g) O-M1D-O2D 0.1–0.1 wt% DI.

2.4. Characterization

Raman spectroscopy was carried out using a Witec 300 Raman microscope with a 532 nm laser (resolution of 1 cm^{-1}). For Raman mapping, images were obtained by integrating the G band in a quadrate region (50 × 50 μm^2) from the fracture zones. DMA was performed on a Perkin Elmer DMA 8000 in a dual cantilever clamp and in multi-frequency mode. The measurements were carried at 1 Hz with a heating rate of 10 °C min^{-1} from room temperature to 150 °C. Sample dimensions were 35 mm × 10 mm × 3.2 mm according to ASTM D4065. Eq. (1) was used to calculate the crosslinking density (ν_e) in the epoxy [32–35] and carbon-reinforced nanocomposites [36]. E_{msm} is the minimum storage modulus, T is the temperature at the rubbery plateau zone, and R is the ideal gas constant.

$$\nu_e = E_{msm}/3RT \quad (1)$$

Images of thin slices of the nanocomposites cut by a microtome were acquired by transmission electron microscopy (JEOL JEM-1010) at a voltage of 80 kV. For the electrical measurements, the two tips method was used. The SPA B1500A equipment provided current versus voltage curves. An electro-sputtering Denton Vacuum Desk V with a silver target was used to prepare samples for electrical measurements for 60 s. The silver was deposited on one face with a 35 mm × 10 mm dimension for the DI nanocomposites and on one face with a 35 mm × 3.2 mm dimension for the LA nanocomposites. A longitudinal space of ~2 mm was left to install the equipment probes in the specimen center.

3. Results and discussion

3.1. Raman spectroscopy

The Raman spectra of the nanocomposites present significant differences for the epoxy. Fig. 2 shows evident shifts and widening of signals at approximately 1235, 1254, 1303, and 1584 cm^{-1}, which correspond to the radial breathing mode (RBM) of aromatics rings [37,38], stretching of the ring-O bond [39,40], in-plane ring mode [41], and ring stretching of the para-di-substituted aromatic [42], respectively.

The full width half maximun (FWHM) of the stretching mode of both the ring-O bond and para-di-substituted aromatic (1254 cm^{-1} and 1584 cm^{-1}) show a broadening in the composites with carbon nanoreinforcements. For the nanocomposites with hybrid 1D-2D reinforcement, the values of the FWHM tend to be higher, only below some signals of the M1D 0.1 wt% DI. However, for the para-disubstituted benzene (1584 cm^{-1}) signal, the FWHM values of the hybrid nanocomposites are above the rest (Table 2). This change on the signals can result from the interaction of the carbon nanostructures and the polymeric chains. Hence, the collective response originates from the electronic clouds that modify the Raman signal [43]. Dresselhaus et al. [44] related the Raman signals to the Van der Waals forces existing in the carbon-carbon nanostructures and carbon-polymeric chains. In this research, the hybrid nanostructures influence the interactions.

Besides, a different arrangement or disorder in the polymeric chains influenced by the nanomaterials could exist [45]. In particular, a strong, marked influence of the π-π interactions can be re-

Table 2
Raman signals of nanocomposites DI.

Vibrational mode / Sample	RBM of aromatic rings		Phenyl-Oxygen (Ether)		1,4 δ in the plane of the benzene ring		Para-disubstituted benzene	
	cm^{-1}	FWHM	cm^{-1}	FWHM	cm^{-1}	FWHM	cm^{-1}	FWHM
Neat epoxy DI	1235	32.8	1254	8.8	1303	35.5	1584	9.6
M1D 0.1 wt% DI	1226	42.3	1252	9.9	1298	35.3	1591	7.4
O-M1D 0.1 wt% DI	1231	30.6	1254	9	1299	35.8	1583	9.9
O2D 0.1 wt% DI	1231	35.9	1254	7.9	1299	33.3	1582	11
RG2D 0.1 wt% DI	1231	30.5	1254	8.5	1299	35.2	1583	11
M1D-RG2D 0.1–0.1 wt% DI	1228	33	1254	9.4	1301	38.9	1582	11.7
O-M1D-O2D 0.1–0.1 wt% DI	1231	29.1	1254	9.8	1299	36.6	1584	10.9

flected in the Raman signal [46]. For instance, in aromatics rings, the signal related to the "para-di-substituted benzene ring" in M1D 0.1 wt% DI is more influenced. Compared to the other samples, this composite could have more influence because of the aromatic rings present in the pristine nanotubes. The "RBM of aromatic rings" and the "1,4 in-plane ring" mode (around 1235 and 1303 cm^{-1}, respectively) exhibit a redshift. These displacements can be associated with the axial deformation of the C–C bond under load and dispersion of the nanostructures, as other authors have mentioned [47,48]. Paipetis [48] reported that the interfacial stress transferred from the epoxy matrix to the nanomaterials produces signal shifts and broadening in the Raman peaks.

Wang et al. [49] reported the modification in the Raman signals due to the interaction of carbon nanostructures and liquid crystals. They made a comparison between two liquid crystals either with or without aromatic rings present in their structure. Their results exhibited changes in the Raman spectra for the first one and no variations in the second case. This observation can be attributed to the aromatic ring structure of materials where the strong π-π interaction exists.

3.2. Raman mapping

The impact strength and the Scanning Electron Microscopy (SEM) analysis of these composites were analyzed in-depth in a previous report [27]. The observations of SEM fractography provided visual details of the fracture front displacement and patterns. However, the density and distribution of nanomaterials could only be analyzed indirectly. Here, the fracture analysis of the of epoxy influenced by carbon reinforcements produces significant differences in the Raman mapping depending on the reinforcement content and dispersion; thus, the Raman mapping detects specific signals of sp^2 carbon allotropes, such as the D or G bands. In this way, the polymeric samples are analyzed faster and with a high degree of correlation to SEM, as has been reported by other authors [50].

Fig. 3a shows a confocal image of the fracture surface, which corresponds to the nanocomposite M1D-RG2D 0.5–0.5 wt% DI. The presence of V and river patterns points to an alteration in the mechanism due to absorbed fracture energy by nanocomposites, after the addition of sp^2 carbon allotropes. Hence, the patterns suggest plastic strain during fracture. Therefore, the area observed in the confocal image was selected for Raman mapping analysis. First, the surface was scanned for the typical carbon nanomaterial signals. Then, the signal characteristics of carbon identified by the Raman spectroscopy allowed for the creation of a 2D image. It is necessary to mention that the objective is mainly to identify areas with a higher density of nanomaterials.

Fig. 3b shows the Raman spectra from a region with a large amount of nanoreinforcements (red spectrum) and a small amount of nanoreinforcements (blue spectrum). Both are based on the G signal intensity from carbon nanomaterials. The Raman mapping allows us to obtain images of the fracture zone at different depths, integrating the region between 1565 and 1610 cm^{-1} (as Fig. 3c illustrates). Also, stacking the images from different Z-axis positions of the fracture surface results in a 3D reconstruction, as Fig. 3d shows, as other authors have reported for some materials [51,52].

According to the reinforcement added, Fig. 4 shows the fracture surface differences. Red and blue zones in the 2D images represent the highest agglomeration and the absence of carbon reinforcements, respectively. Fig. 4a corresponds to neat epoxy DI; this picture shows a smooth and mirror-like surface with confocal microscopy. Consequently, its Raman mapping does not show the G band activity, resulting in a smooth mapping as shown by the 2D and 3D views (the minor presence of blue and red dots can be attributed to the noise generated during the testing of the materials, not to the nanomaterials). For the M1D 0.5 wt% DI nanocomposite (Fig. 4b), the 2D and 3D maps showed activity for the signal of 1D reinforcement even when the confocal image does not show plastic strain patterns.

In Fig. 4b, 1D agglomerations can be observed as a Raman mapping evidenced in red zones. Besides, the blue zones reveal the limited presence of carbon nanomaterials in some regions, affecting the mechanical performance. Raman mapping reveals the material composition, pointing to carbon agglomerations that confocal microscopy could not detect. 3D reconstruction gives an extra non-destructive tool to study the spatial distribution of the carbon nanomaterials, as exhibited in Fig. 4.

Figs. 4c-d reveal correlations between the relief in the fracture patterns (confocal image) and the highest concentrated carbon nanomaterial regions. The superposition of the 2D Raman map over the confocal image exhibits the same pattern. This result supports the fact that the nanostructures deviate from the fracture front. Samples RG2D 0.5 wt% DI and M1D-RG2D 0.5–0.5 wt% DI improve the Raman mapping analysis due to the high presence of sp^2 nanostructures. Consequently, it provides evidence of agglomeration and empty zones. This behavior is not exclusive to these two samples; all nanocomposites exhibited a similar response in this analysis. This characterization technique offers an alternative analysis tool to complete the fracture surface study, as shown in Fig. 4b-c.

3.3. Dynamical mechanical analysis

3.3.1. Glassy state of DI nanocomposites

Fig. 5 shows the behavior of the storage modulus (E') versus temperature. The results exhibit a different response of E' at 37 °C after adding reinforcements 1D, 2D, or the blends 1D-2D to the epoxy matrix.

The E' values at 37 °C for hybrid multidimensional nanocomposites (O-M1D-O2D 0.1–0.1 wt% DI and M1D-RG2D 0.1–0.1 wt% DI) are higher in comparison to the rest of nanocomposites. Other works [10,23,26,27,53-61] report (Table 3) that the combination of sp^2 carbon allotropes generates this kind of improvement because of a synergistic effect between nanostructures.

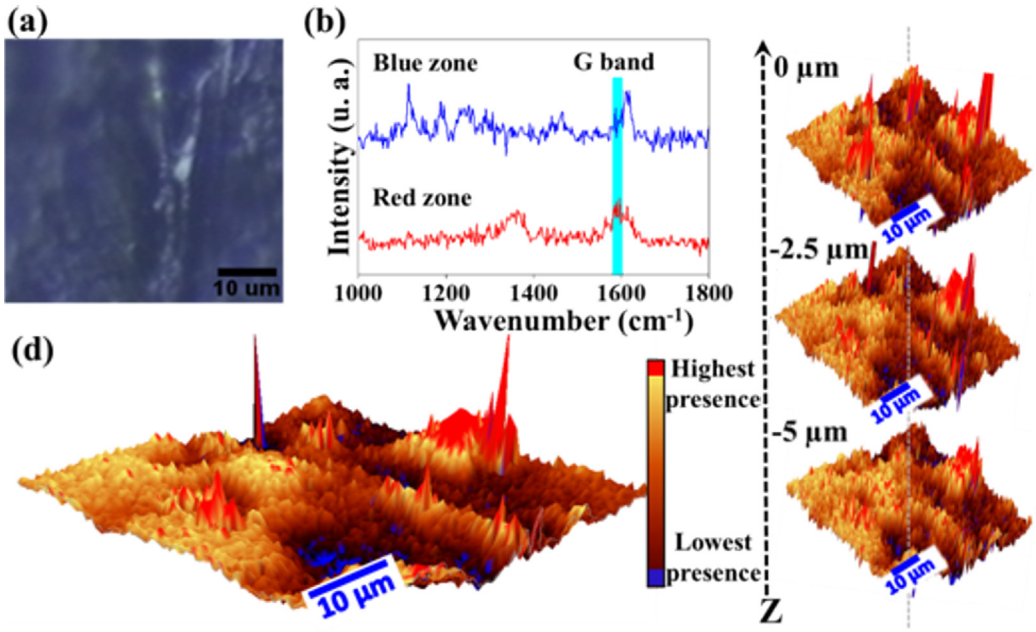

Fig. 3. (a) Confocal micrograph of the fracture surface of M1D-RG2D 0.5–0.5 wt% DI nanocomposite; (b) Raman spectrum nanocomposite from the red and blue zones in Raman mapping; (c) integration maps based on G band of carbon nanoreinforcement; (d) reconstructed 3D zone of the fracture surface of M1D-RG2D 0.5–0.5 wt% DI nanocomposite.

Li and Wang 2019 [62] reviewed the literature on hybrid nanostructures for energy storage and conversion. In that work, they classified core/shell, cactus-like, and sandwich-like 1D-2D hybrid nanomaterials. In the case of the sandwich-like 1D-2D nanomaterials, synergized nanostructures (SLN) are described as well-dispersed 1D nanomaterials incorporated into the 2D layer-structured materials. Hence, the improvements in the electrical and mechanical features in nanocomposites are originating from the SLN, and the 2D sheets perturbed by 1D nanostructures to prevent agglomerations is mentioned as a key factor [62]. Consequently, the continuous network formed by 1D-2D nanostructures is favorable for fast electron transfer. Moreover, the resulting large specific surface area of interconnected 1D-2D nanostructures is also available to form enriched interphases, either physical or chemical (depending on the reinforcement), with the matrix.

According to Table 3, the thermomechanical response of 1D-2D nanocomposites has been scarcely studied. Hence, to explain the viscoelastic response of 1D-2D nanocomposites, parameters such as the reinforcement concentration need to be studied in detail. In the present research, we focused on the effect of the concentrations shown in Table 1. Also, a comparison among the non-functionalized and functionalized nanomaterials used to obtain 1D-2D hybrid carbon nanomaterials and their impact on E' was carried out. A comparison of our findings with another research was established. It is determined that the 1D-2D hybrid reinforcement effect (SLN) was similar to that described by Li and Wang (2019). From this type of reinforcement, E' in some hybrid reinforced nanocomposites showed a stiffness of almost twice the value at a glassy state compared to the epoxy matrix. Moreover, the T_g exhibited displacements to higher temperatures compared to the polymeric matrix.

The results obtained in this work also coincide with those reported by Jen and Huang [60], who compared the properties of a reinforced nanocomposite with a concentration fixed at 4 wt% of a 1D-2D hybrid in different ratios (Table 3); the best ratio obtained for 1D and 2D was 1:9. The fixed concentration proposed by the authors [60] was based on previous reports and considering the tensile response but only at room temperature. In other research, Im and Kim [26] observed an increase in the E' during DMA analysis for temperatures above T_g due to the 1D-2D reinforcement. E' for the matrix was initially above the nanocomposites until approximately the T_g value, where the 1D-2D nanocomposite changed to high E' values. In this case, the reinforcement percent added was 50 wt% because of the synthesis method. In the study published by Shen et al. [58], the E' values are not reported. Instead, they focus their discussion on the increase in the T_g due to the SLN effect from 1D-2D reinforcement. These results match with those observed in our research for T_g; however, this topic is discussed later.

Table 4 shows the parameters E' and T_g generated by DMA. The hybrids show a higher E' compared with the rest of the nanocomposites. This behavior suggests that the packing of 2D nanomaterials is disturbed by M1D. Simultaneously, 2D nanoreinforcements offer ample planar geometry to interact with the 1D nanomaterials to form 3D hybrid structures [26]. In other words, the available area to form an interface amongst the epoxy resin and nanoreinforcements increased considerably. Additionally, π-π interactions amongst the 1D & 2D nanostructures give an extra restriction effect to polymeric chains [8,54,63,64], impacting the E' values. The high E' values even at low percentages of carbon added point to well-dispersed reinforcements, as other authors have mentioned [65,66].

The existence of oxygenated moieties in reinforcements favors the intercalation among 1D & 2D materials promoting different interactions [7-10, 14-18]. Consequently, nanostructures can cause an increase in the stiffness of the epoxy resin. This response is emphasized in the blends with O-M1D, as the results show [67].

Fig. 6 shows E' thermograms of neat epoxy DI and nanocomposites O-M1D-O2D and O-M1D-RG2D. In this figure, the whole composites exhibit the highest E' compared to the neat epoxy DI in both the glassy and the rubbery plateau. For the O-M1D-O2D nanocomposites, the storage modulus diminishes as the 2D reinforcement increases. As Montazeri et al. [65] commented, it can be attributed to the formation of agglomerates. As the results suggest, the agglomerates inhibit the synergistic effect between the blend of the 1D & 2D nanostructures.

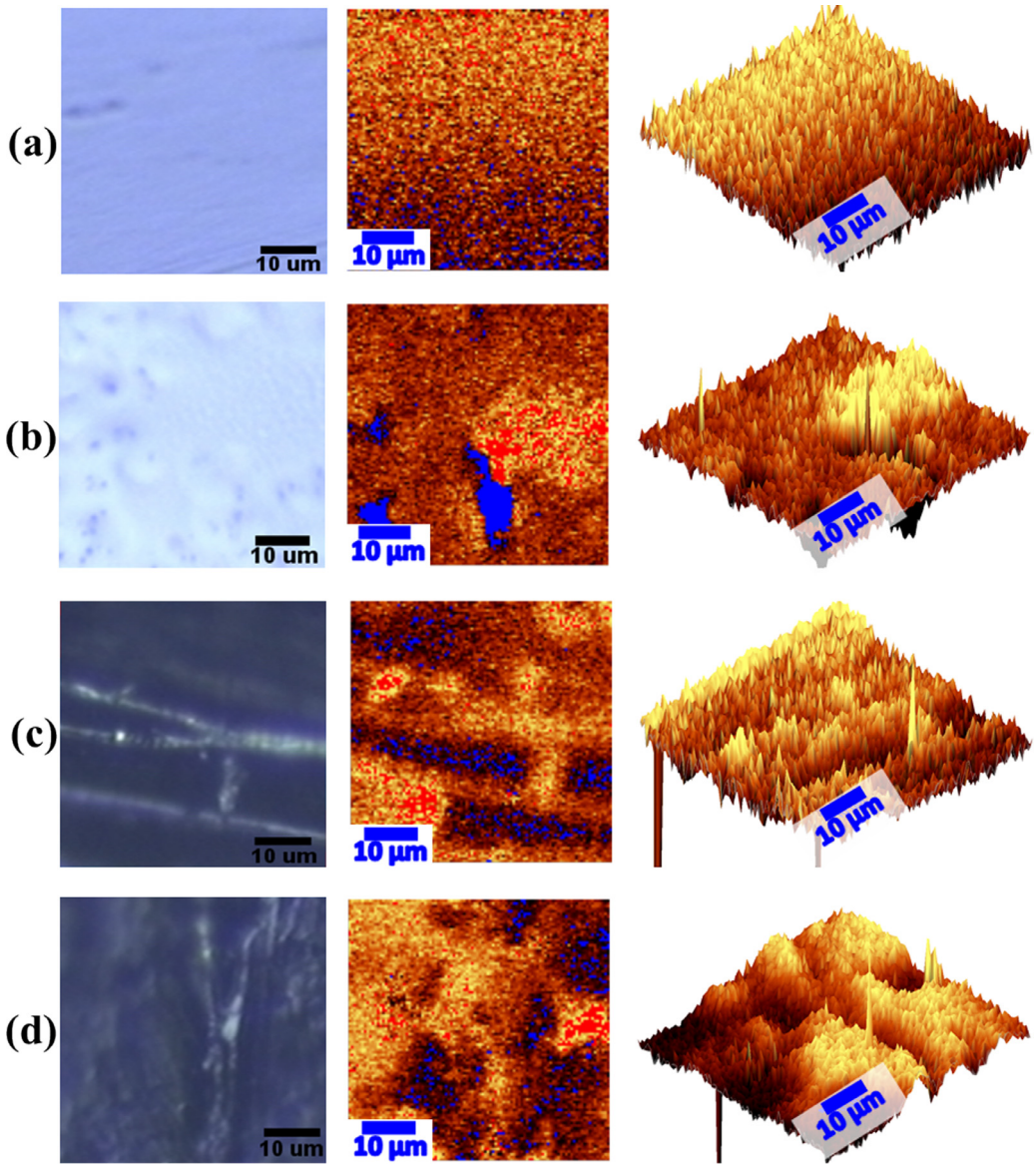

Fig. 4. Raman fracture analysis of epoxy matrix and DI nancomposites. Confocal images of fracture surface zones (left), Raman mapping of fracture surface built from G band of carbon reinforcements (center) and 3D Raman image (right) obtained from (a) Neat epoxy DI; (b) M1D 0.5 wt% DI; (c) RG2D 0.5 wt% DI; (d) M1D-RG2D 0.5–0.5 wt% DI nanocomposites (the red and blue zones showed the highest and the lowest presence of carbon reinforcements).

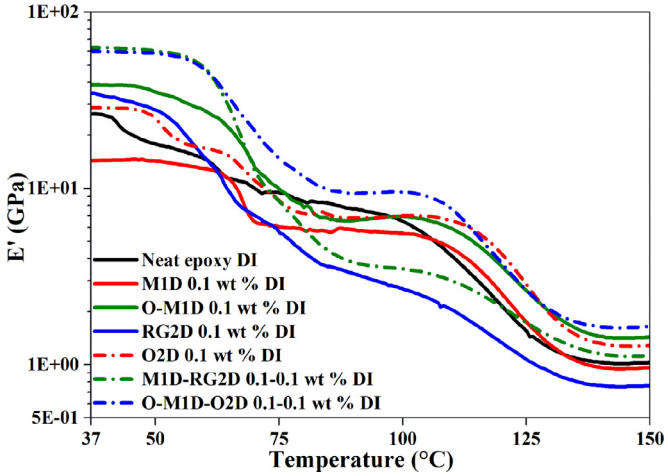

Fig. 5. DMA results (E' vs. temperature) of the neat epoxy DI and nanocomposites DI.

The viscoelastic response depends on parameters such as dispersion obtained, the quantity of reinforcement, geometrical characteristics of nanostructures (dimension), and the interfaces of the polymer-reinforcement and reinforcement–reinforcement [7,68]. Combining these parameters promotes better interaction of the O-M1D-O2D blend at a low amount of 2D reinforcement. Meanwhile, RG2D nanocomposites require a high amount of 2D reinforcement in the mixture to obtain a high storage modulus.

Table 4 shows the values obtained for the crosslinking density. It is observed that adding the sp^2 nanomaterials impacts the reaction of the epoxy crosslink. The crosslinking density (ν_e) is related proportionally to the rubbery modulus. Hence, the general elastic response depends directly on the ν_e in epoxy-based nanocomposites.

For the neat epoxy DI, the ν_e is 0.97 mol m^{-3}. For the composites with oxidized nanomaterials, the ν_e for O-M1D 0.1 wt% DI and O2D 0.1 wt% DI is higher than epoxy DI. In contrast, when unoxidized nanomaterials are added at the same concentrations (RG2D 0.1 wt% DI and M1D 0.1 wt% DI), the ν_e values decrease. The RG2D

Table 3
Hybrid epoxy-based nanocomposites reinforced with sp^2 carbon allotropes.

Reinforcement 1D-2D	Reinforcement (%)	Mechanical properties	Dispersion method	λ (W $m^{-1}K^{-1}$)	σ (S m^{-1})	E' (Pa) T_g (°C)	Raman	Reference
M1D -MGPs	Ratio 0.1:0.9 at 1 wt%	3350 MPa Tensile modulus 65 Mpa Tensile Strenght	US	0.321	~	~	One point	[53]
M1D-O2D	Ratio 49.52–0.48 at 50 wt%	~	Wetting procces	3	~	E'≈3 × 10^9 T_g≈100 °C	~	[26]
M1D-GNPT	Ratio 9:1 at 0.5 wt%	3.1 GPa Flexural modulus	TRM	0.7	~	~	~	[54]
M1D –GNPT	Ratio 1:1 at 5 wt%	~	US	0.45	10^{-2}	~	~	[55]
M1D –GN	Ratio 1:1 at 3 wt%	148 KPa Tensile modulus	US	~	~	~	~	[56]
M1D–GNPT	Ratio 8:2 at 0.8 wt%	~	Simultaneous US-magnetic stirring	~	10^{-6}	~	~	[57]
M1D-O2D	Ratio 0.5–0.1 phr	~	US	~	~	T_g≈158 °C	~	[58]
M1D –GNPT	Ratio 3:1 at 6.1 wt%	~	US	0.9	10^{-7}	~	~	[23]
M1D –GNP	Ratio 0.1:0.4 at 0.5 vol%	3000 MPa Tensile modulus 2500 MPa Tensile strenght	US	~	10^{-1} (at 0.8 vol%; ratio 0.1:0.4)	~	~	[10]
O-M1D-O2D	0.1 wt% –0.5 wt%	Impact resistance 5.84 KJm^{-2}	US	~	~	~	~	[27]
A_{f-}M1D-A_{f-}MLG	Ratio 1:1 at 1 wt%	2900 MPa Tensile modulus 2302 MPa Flexural modulus 3217 MPa Tensile strenght 49 MPa Flexural stress199.4	US	~	~	~	~	[59]
M1D-GNPT	Fixed at 4 wt% with ratios of 0:10, 10:0, 1:9, 3:7, 5:5, 7:3, and 9:1	~	US	~		E'≈1.6 × 10^9 T_g≈98 °C	~	[60]
M1D-O2D	Ratio 5:1 or 0.2 wt% –0.04 wt%	2.35 MPa Tensile modulus 50 MPa Tensile strenght	US	~	~	~	~	[61]
O-M1D-O2D	0.1 wt% –0.1 wt%	~	US	~	10^{-5}	E'≈59.89 × 10^9 T_g≈118 °C	Mapping	This work

Abbreviations: M1D, Multi-walled carbon nanotubes; O-M1D, Oxidized multi-walled carbon nanotubes; GNPT, Graphene nanoplatelets; GN, Graphene; O2D, Graphene oxide; RG2D, Reduced graphene oxide; GNP, Graphene nanopowder; A_{f-}MLG, Amino functionalized multilayer graphene; A_{f-}M1D, Amino functionalized M1D; MGPs, Multigraphene platelets; TRM, Three roll mill; US, Ultrasound; E', Storage modulus; T_g, Glass transition temperature; λ, Thermal conductivity; σ, Electrical conductivity.

is considered an "unoxidized" material given the reduction reaction, which separates most of the oxygenated moieties in O2D. Thus, the ν_e results shown alterations in the crosslinking of the nanocomposite caused by the covalent bonds among the reinforcement and matrix [17,63,68-71]. Besides, the interaction amongst polymeric chains surrounded by nanomaterials (secondary interactions) can be achieved, as other authors have mentioned [67–71].

3.3.2. Glass transition of DI nanocomposites

Fig. 7 shows the damping curves of neat epoxy DI and the DI nanocomposites. The maximum in the Tan δ curve represents the temperature at which the glass transition occurs. After deconvolution of the peak, the Tan δ curve shows two signals registered in Table 4. The first one corresponds to a glass transition temperature (T_g) of the material partially cured (T_{gp}) and the second one to a fully cured material ($T_{g\infty}$) [70]. Monomer variation, an irregular mix between EDA-DGEBA, and oxygenated moieties can influence the cured state, inducing a second phase in the polymer [72–73].

Also, Fig. 7 shows tan δ peak positions. Nanocomposites show peaks of the tan δ at a higher temperature than the epoxy. This change suggests better thermomechanical stability and stiffening effect in nanocomposites [67]. Less movement of polymeric chains produces shifts to high temperatures. Also, a high crosslinking encourages decreased T_g peak height [74]. Hence, the E' of nanocomposites is at least two times higher than the E' of neat epoxy DI, which indicates improvements in the elastic response.

Fig. 8 shows Tan δ signals of neat epoxy DI and nanocomposites (O-M1D-O2D 0.1–0.1 wt% DI, O-M1D-RG2D 0.1–0.1 wt% DI, O-M1D-O2D 0.1–0.5 wt% DI, and O-M1D-RG2D 0.1–0.5 wt% DI). The whole composites exhibit shifts in their $T_{g\infty}$ to higher temperatures compared to neat epoxy DI. The polymeric chain movements are less in these nanocomposites than in pure epoxy, evidencing changes in the viscoelastic performance [26,57,58,64]. Gu et al. [75] attributed the T_g shifts to higher temperatures to the increase in the volume of confined polymer segments. In other words, if the confinement points increase, the relaxation of polymer segments decreases. Hence, T_g will be observed at higher temperatures. Furthermore, the oxygenated moieties over carbon nanostructures improve the affinity of 1D & 2D nanostructures with the epoxy matrix and the dispersion acquired for the O-M1D-O2D blends [17,20].

3.3.3. Glassy state of LA nanocomposites

Table 4 shows that most LA nanocomposites have a higher performance than the neat epoxy LA. In the results of materials O-M1D-O2D 0.1–0.1 wt% LA and O-M1D-RG2D 0.1–0.5 wt% LA, E' increases around 63% and 50%, respectively, in comparison to the

Table 4
Parameters obtained from DMA measurements of nanocomposites DI and nanocomposites LA.

	E' at room temperature (GPa)	% increment of E' at room temperature	Peak 1 T_{gp} (°C)	Peak 2 T_g (°C)	Crosslinking density ν_e (mol m^{-3})
Neat epoxy DI	26.42	Does not apply	84	115	0.097
M1D 0.1 wt% DI	14.31	−46	90	121	0.090
O-M1D 0.1 wt% DI-	38.59	46	86	122	0.135
O2D 0.1 wt% DI	28.74	9	89	125	0.121
RG2D 0.1 wt% DI	34.72	31	86	122	0.072
M1D-RG2D 0.1–0.1 wt% DI	62.86	138	83	112	0.106
O-M1D-O2D 0.1–0.1 wt% DI	59.89	127	86	118	0.155
O-M1D-O2D 0.1–0.5 wt% DI	38.05	44	93	121	0.159
O-M1D-RG2D 0.1–0.1 wt% DI	36.5	38	84	120	0.126
O-M1D-RG2D 0.1–0.5 wt% DI	50.49	91	87	120	0.146
Neat epoxy LA	18.2	Does not apply	82	116	0.073
M1D 0.1 wt% LA	28.2	55	81	115	0.084
O-M1D 0.1 wt% LA	21.19	16.5	83	115	0.105
O2D 0.1 wt% LA	19.63	8	80	116	0.074
RG2D 0.1 wt% LA	19.23	6	83	118	0.090
O-M1D-RG2D 0.1–0.1 wt% LA	27.24	50	83	117	0.120
O-M1D-O2D 0.1–0.1 wt% LA	29.57	63	82	110	0.086

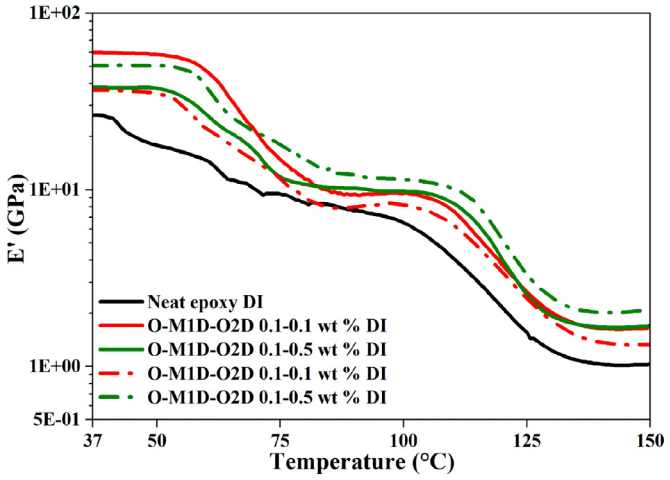

Fig. 6. Thermograms of DMA results (E' vs. temperature) of the neat epoxy DI and nanocomposites DI of samples reinforced with O-M1D and 2D nanomaterials.

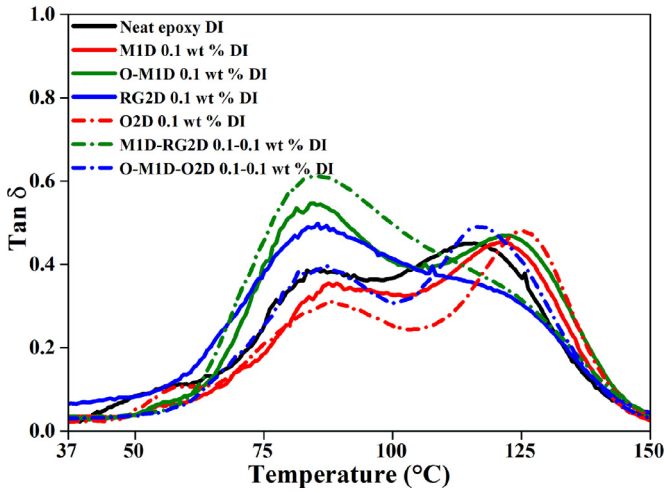

Fig. 7. Tan δ curves of neat epoxy DI and nanocomposites DI reinforced with 1D & 2D materials.

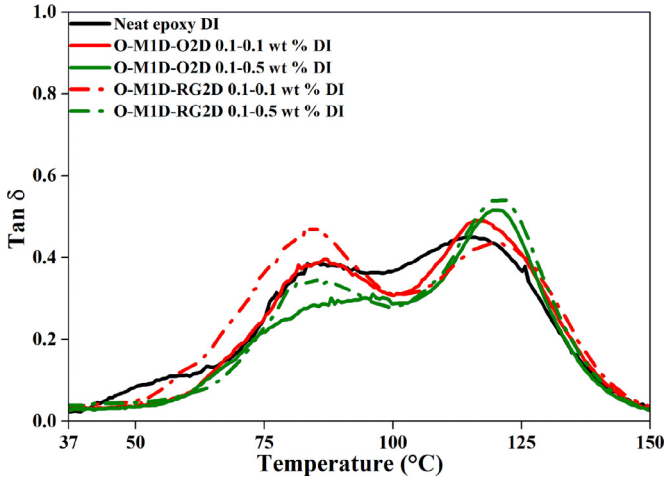

Fig. 8. Tan δ curves of neat epoxy and nanocomposites DI reinforced with O-M1D and 2D nanomaterials.

epoxy matrix. This increase occurs despite the interface between the layers of multilayer nanocomposites. It can be related to the amount of polymer used in each layer of the nanocomposites LA, allowing better dispersion in the ultrasonic bath. Consequently, the impact of the additional interface between polymer layers is diminished. Hence, the final thermomechanical properties obtained from intercalating epoxy-1D and epoxy-2D can be explained as an indirect hybrid effect (not direct as in 1D-2D DI composites). For the O-M1D-O2D 0.1–0.1 wt% LA nanocomposite, the E' value (29.57 GPa) links the presence of moieties groups with the high performance in the viscoelastic properties. The oxygenated moieties contribute to the affinity and dispersion amongst the carbon nanomaterials and epoxy [76].

3.3.4. Glass transition of LA nanocomposites

Tan δ values in multilayer nanocomposites and epoxy LA show minimal differences (Table 4). This behavior indicates that the carbon nanomaterials have a minimal influence on the epoxy crosslinking reaction. The ν_e parameter in LA nanocomposites

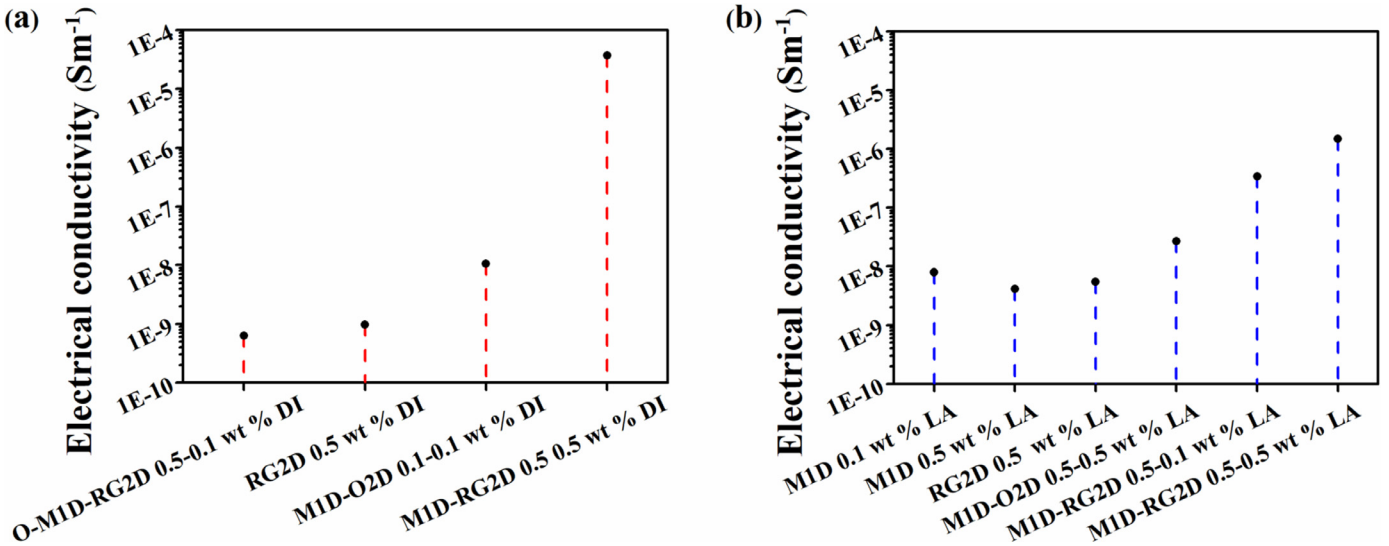

Fig. 9. The electrical conductivity of (a) nanocomposites DI, and (b) nanocomposites LA.

showed less influence on the T_g value of carbon nanoreinforcements than the nanocomposites DI. The slight amount of carbon nanostructures dispersed in the LA nanocomposites avoids the strong influence on the stoichiometry of the cure reaction [77,78]. Moreover, the order of stacking 1D-2D layers shows a strong influence on the final properties of the nanocomposites, as the results suggest.

3.3.5. Electrical response of hybrid nanocomposites

Fig. 9 shows the electrical conductivity (σ) of DI nanocomposites and LA nanocomposites. The conductivity was calculated from the current-voltage curve slope. Thus, the values in Fig. 9 are for the samples that show this curve. The rest of the nanocomposites exhibit a chaotic pattern in the measurements. For the epoxy matrix, some authors [79,80] have reported typical values for σ of around 10^{-12} S m^{-1}. For nanocomposites DI, the blends with either M1D or RG2D exhibit changes in the electrical response. However, for the sample M1D 0.1 wt% DI, no conductivity signal was detected (which explains its omission in Fig. 9). Therefore, the results suggest that the nanomaterials added in this sample are not enough to modify the electrical properties. Even though the mechanical properties indicate good dispersion, this concentration does not reach the percolation threshold for electrical conductivity.

The nanocomposites O-M1D-RG2D 0.5–0.1 wt%, and RG2D 0.5 wt% exhibited a slight change in the electrical properties compared to the epoxy. Both nanocomposites show similar conductivity but with different amounts of RG2D. For the material with 1D-2D hybrid reinforcement, it can be inferred that the dispersion improves with the addition of the 1D materials. Therefore, less amount of RG2D can generate the electrical conduction network. These results are similar to those reported by Jen & Huang [60], who observed that the best filler ratio was 9:1 in a 10% hybrid M1D and GNPT. The response observed is attributed to the synergetic effect from two geometrically different carbon nano-fillers. In other words, the M1D built bridges between GNPT, preventing the agglomeration and enhancing the dispersion of 2D nanomaterials. Jen & Huang [60] mentioned the filler ratio on hybrid nanocomposites needs to be studied. Hence, the hybrid reinforcement offers a wide field of study where issues such as interaction with matrix (compatibility), agglomerations of 1D, stacking of 2D, and strategies of functionalization have not yet been resolved [81].

For the LA nanocomposites, the values of σ exhibit some differences compared to the DI nanocomposites (Fig. 9b). The results suggest that the non-oxidized reinforcements and the dispersion in each layer encourage change in the electrical response. Similar to the viscoelastic response, an indirect hybrid response in the nanocomposite M1D-RG2D 0.5–0.5 wt% LA produces the highest σ (1.47×10^{-6} S m^{-1}). In contrast, the σ for the nanocomposites with one nanomaterial, such as M1D 0.5 wt% LA and RG2D 0.5 wt% LA, is 4.11×10^{-9} and 5.41×10^{-9} S m^{-1}, respectively.

3.3.6. Microstructure of nanocomposites at cured state

Thin slices of nanocomposites were analyzed with TEM to investigate the dispersion of carbon nanostructures into the epoxy matrix. Fig. 10a-b shows the distribution of carbon nanostructures in the epoxy matrix. Fig. 10a shows that 1D carbon materials distribute randomly on the epoxy composite for the composite O-M1D 0.1 wt% DI. Distribution affects the mechanisms of reinforcement, consequently impacting the properties of nanocomposites with M1D [82,83]. For the sample RG2D 0.1 wt% DI (Fig. 10b), irregular and wrinkle flakes dispersed on the epoxy can be observed.

The thermomechanical properties suggest a synergetic effect of 1D & 2D nanoreinforcements for some nanocomposites. There is no evidence of a correlation between the quantity of nanomaterials added and mechanical performance. However, as E' exhibits in some blends, there is the possibility that the combination of reinforcements and their subsequent carbon-carbon and carbon-epoxy interactions support the improvements. The latter is due to the synergy of carbon reinforcements over the epoxy as a network among 3D hybrid nanostructures, as other authors have mentioned [23,25,57]. Charitos et al. [84] reported a synergistic effect among M1D-O2D in a linear low-density polyethylene (LLDPE) matrix. They mentioned that the synergistic effect of the carbon nanomaterials leads to a decreased percolation threshold of electrical conductivity. The intercalation of M1D into the O2D bridges the 2D reinforcement, as described by Li and Wang in 2019 [62] for SLN, and then a conductive path is formed in the matrix. In this work, a hybrid bridging mechanism was formed, as the TEM images suggest, (which was previously mentioned), (Fig. 10c-f). Consequently, the resulting interconnected network in DI nanocomposites is the principal factor in the mechanical and electrical changes.

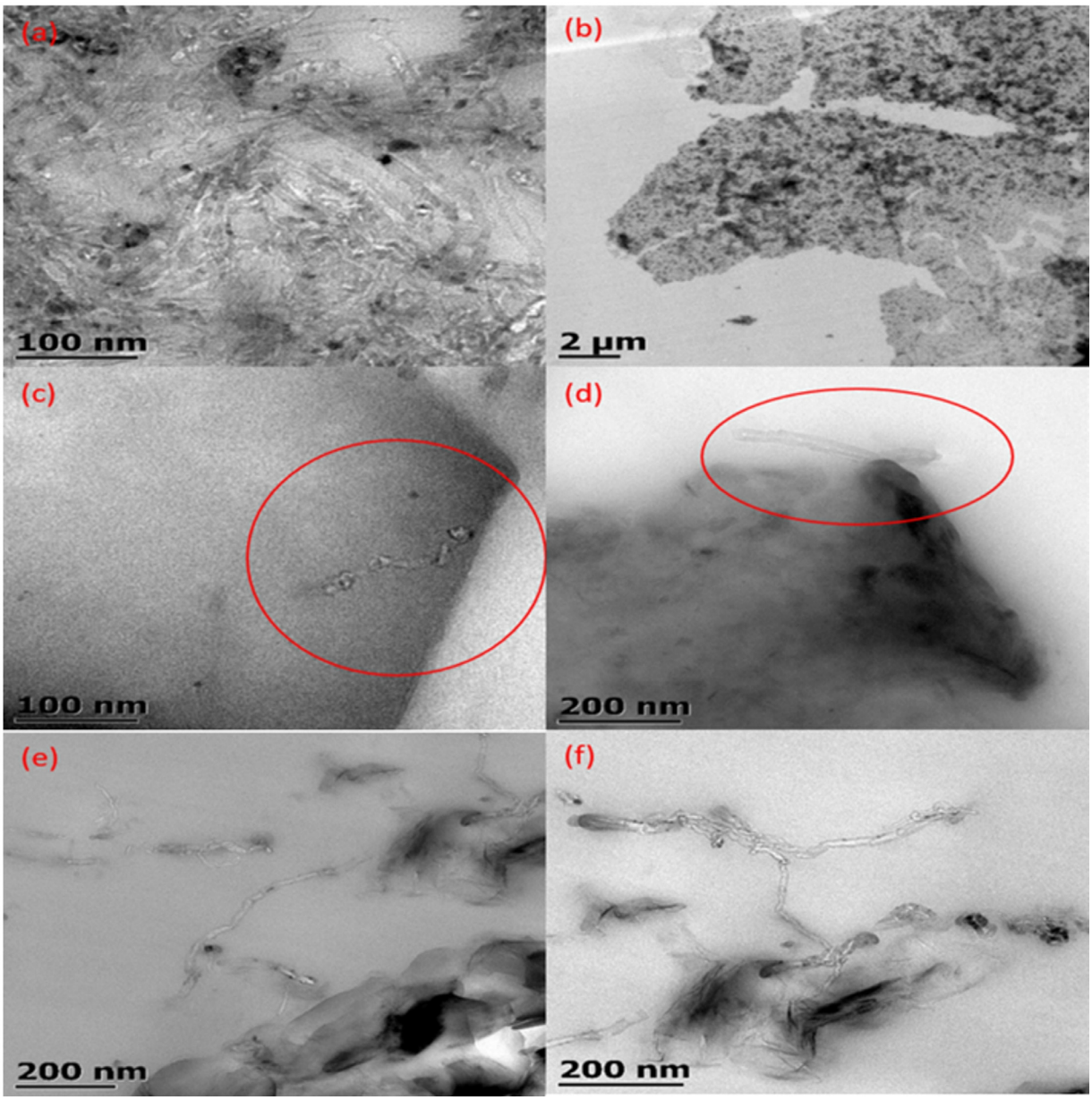

Fig. 10. TEM micrographs of nanocomposites (a) O-M1D 0.1 wt% DI; (b) RG2D 0.1 wt% DI; (c) O-M1D-O2D 0.1–0.1 wt% DI; (d) M1D-RG2D 0.1–0.1 wt% DI; (e-f) M1D-RG2D 0.5–0.5 wt% DI.

4. Conclusions

The hybrid 1D-2D carbon reinforcement on nanocomposites and their thermomechanical and electrical performance have been investigated. 1D-2D reinforcements were obtained from the combination of unoxidized and oxidized carbon nanomaterials at different concentrations. The combination of O-M1D and O2D showed the influence of functional groups on the dispersion and distribution of nanoreinforcements into the matrix. Moreover, the oxidized carbon nanomaterials improve the compatibility with the matrix, as implied by the ν_e values. Then, the nanocomposites with hybrid reinforcement reflect the higher E' values.

Raman mapping showed that the spatial distribution of carbon nanomaterials in the fracture surfaces match with the river patterns. This fact is a clear signal that the carbon nanomaterials influence the change in the brittle nature of the polymeric matrix. TEM micrographs of DI nanocomposites showed the zones of 3D networks created from the 1D-2D carbon materials. Based on the two different geometries of graphene-based materials, this interconnected network causes mechanisms of hybrid reinforcement. The electrical conductivity of the nanocomposites provides additional evidence of the synergistic effect originated between carbon nanomaterials. In this test, the conductivity of the hybrid nanocomposite increases by around four orders of magnitude compared to materials with only one kind of nanomaterial. The 1D-2D hybrid provides a route to synthesize multifunctional nanocomposites at low amounts of carbon materials.

Declaration of Competing Interest

The authors declare that they have no known competing financial interests or personal relationships that could have appeared to influence the work reported in this paper.

CRediT authorship contribution statement

J. López-Barroso: Methodology, Validation, Formal analysis, Investigation, Writing – original draft, Visualization. **A.L. Martínez-Hernández:** Conceptualization, Resources, Writing – review & editing, Supervision, Project administration. **J.L. Rivera-Armenta:** Resources, Writing – review & editing, Supervision, Project administration. **A. Almendárez-Camarillo:** Resources, Writing – review & editing, Supervision. **P.E. García-Casillas:** Resources, Writing – review & editing, Supervision, Project administration, Funding acquisition. **C.G. Flores-Hernández:** Investigation, Writing – original draft, Visualization. **C. Velasco-Santos:** Conceptualization, Resources, Writing – review & editing, Supervision, Project administration, Funding acquisition.

Acknowledgments

The authors thank the Neurobiology Institute of the National Autonomous University of Mexico (UNAM) and the BE Maria de Lourdes Palma-Tirado to support microtome cuts and acquire TEM micrographs. Also, to the Autonomous University of Ciudad Juarez (UACJ), especially to Dr. Abimael Jiménez-Pérez for his assistance on the electrical measurements and Dr. Rurik Farías-Mancilla for his support on the Raman spectroscopy. To TecNM for the Supported Project 10126.21-P. The authors are also thankful to the National Laboratory of Graphenic Materials for support. J. López-Barroso is grateful to the National Council for Science and Technology of Mexico (CONACYT) for the Ph.D. Grant. 435347 and, to Composites Network (MATCORED) to support mobility.

References

[1] A.C. Ferrari, Raman spectroscopy of graphene and graphite: disorder, electron-phonon coupling, doping and nonadiabatic effects, Solid State Commun. 143 (2007) 47–57, doi:10.1016/j.ssc.2007.03.052.
[2] V. Kumar, J.Y. Lee, D.J. Lee, Synergistic effects of hybrid carbon nanomaterials in room-temperature-vulcanized silicone rubber, Polym. Int. 66 (2017) 450–458, doi:10.1002/pi.5283.
[3] S. Roy, S.K. Srivastava, J. Pionteck, V. Mittal, Assembly of layered double hydroxide on multi-walled carbon nanotubes as reinforcing hybrid nanofiller in thermoplastic polyurethane/nitrile butadiene rubber blends, Polym. Int. 65 (2016) 93–101, doi:10.1002/pi.5032.
[4] H. Lu, K. Yu, S. Sun, Y. Liu, J. Leng, Mechanical and shape-memory behavior of shape-memory polymer composites with hybrid fillers, Polym. Int. 59 (2010) 766–771, doi:10.1002/pi.2785.
[5] D.G. Papageorgiou, I.A. Kinloch, R.J. Young, Mechanical properties of graphene and graphene-based nanocomposites, Prog. Mater. Sci. 90 (2017) 75–127, doi:10.1016/j.pmatsci.2017.07.004.
[6] Q. Ke, J. Wang, Graphene-based materials for supercapacitor electrodes – a review, J. Materiom. 2 (2016) 37–54, doi:10.1016/j.jmat.2016.01.001.
[7] S. Liu S, V.S. Chevali, Z. Xu, D. Hui, H. Wang, A review of extending performance of epoxy resins using carbon nanomaterials, Compos. B Eng. 136 (2018) 197–214, doi:10.1016/j.compositesb.2017.08.020.
[8] U. Szeluga, B. Kumanek, B. Trzebicka, Synergy in hybrid polymer/nanocarbon composites. A review, Comp. Part A App. Sci. Manuf. 73 (2015) 204–231, doi:10.1016/j.compositesa.2015.02.021.
[9] N. Domun, K. Paton, H. Hadavinia, T. Sainsbury, T. Zhang, H. Mohamud, Enhancement of fracture toughness of epoxy nanocomposites by combining nanotubes and nanosheets as fillers, Materials (Basel) 10 (2017) 1179–1196, doi:10.3390/ma10101179.
[10] Z. Ghaleb, M. Mariatti, Z. Ariff, Synergy effects of graphene and multiwalled carbon nanotubes hybrid system on properties of epoxy nanocomposites, J. Reinf. Plast. Compos. 36 (2017) 685–695, doi:10.1177/0731684417692055.
[11] S. Nishimura, N. Narayan, O. Sahin, A.D.S. McWilliams, K.A. Miller, D. Salpekar, Z. Wang, J. Joyner, A.A. Martí, R. Vajtai, M. Ashokkumar, P.M. Ajayan, Luminescent hybrid biocomposite films derived from animal skin waste, Carbon Trends 4 (2021) 100059, doi:10.1016/j.cartre.2021.100059.
[12] N.V. Lakshmi, P. Tambe, N.K. Sahu, Giant permittivity of three phase polymer nanocomposites obtained by modifying hybrid nanofillers with polyvinylpyrrolidone, Compos. Interfaces 25 (2018) 47–67, doi:10.1080/09276440.2017.1338876.
[13] G. Nassar, E. Daou, R. Najjar, M. Bassil, R. Habchi. A review on the current research on graphene-based aerogels and their applications. Carbon trends. 4 (2021) 100065. DOI: https://doi.org/10.1016/j.cartre.2021.100065
[14] C. Lee, X. Wei, J.W. Kysar, J. Hone, Measurement of the elastic properties and intrinsic strength of monolayer graphene, Science 321 (2008) 385–388, doi:10.1126/science.1157996.
[15] V. Singh, D. Joung, L. Zhai, S. Das, S.I. Khondaker, S. Seal, Graphene based materials: past, present and future, Prog. Mater. Sci. 56 (2011) 1178–1271, doi:10.1016/j.pmatsci.2011.03.003.
[16] S. Zhang, S. Yin, C. Rong, P. Huo, Z. Jiang, G. Wang, Synergistic effects of functionalized graphene and functionalized multi-walled carbon nanotubes on the electrical and mechanical properties of poly(ether sulfone) composites, Eur. Polym. J. 49 (2013) 3125–3134, doi:10.1016/j.eurpolymj.2013.07.011.
[17] F.V. Ferreira, F.S. Brito, W. Franceschi, E.A.N. Simonetti, L.S. Cividanes, M. Chipara, K. Lozano, Functionalized graphene oxide as reinforcement in epoxy based nanocomposites, Surf. Interfaces 10 (2018) 100–109, doi:10.1016/j.surfin.2017.12.004.
[18] G. Mittal, V. Dhand, K.Y. Rhee, S.-J. Park, W.R. Lee, A review on carbon nanotubes and graphene as fillers in reinforced polymer nanocomposites, J. Ind. Eng. Chem. 21 (2015) 11–25, doi:10.1016/j.jiec.2014.03.022.
[19] R. Ashwini, Z. Mohanta, M.K. Punith Kumar, M.S. Santosh, C. Srivastava, Enhanced heterogeneous electron transfer kinetics in Graphene Oxide produced from mechanically milled Graphite, Carbon Trends 5 (2021) 100095, doi:10.1016/j.cartre.2021.100095.
[20] Y. Wei, X. Hu, Q. Jiang, Z. Sun, P. Wang, Y. Qiu, W. Liu, Influence of graphene oxide with different oxidation levels on the properties of epoxy composites, Compos. Sci. Technol. 161 (2018) 74–84, doi:10.1016/j.compscitech.2018.04.007.
[21] L.J. Cote, J. Kim, V.C. Tung, J. Luo, F. Kim, J. Huang, Graphene oxide as surfactant sheets, Pure Appl. Chem. 83 (2011) 95–110, doi:10.1351/PAC-CON-10-10-25.
[22] T. Subhani, M. Latif, I. Ahmad, S.A. Rakha, N. Ali, A.A. Khurram, Mechanical performance of epoxy matrix hybrid nanocomposites containing carbon nanotubes and nanodiamonds, Mater. Des. 87 (2015) 436–444, doi:10.1016/j.matdes.2015.08.059.
[23] H.P. Chang, H.C. Liu, C.S. Tan, Using supercritical CO_2-assisted mixing to prepare graphene/carbon nanotube/epoxy nanocomposites, Polymer (Guildf) 75 (2015) 125–133, doi:10.1016/j.polymer.2015.08.023.
[24] W. Li, A. Dichiara, J. Bai, Carbon nanotube-graphene nanoplatelet hybrids as high-performance multifunctional reinforcements in epoxy composites, Compos. Sci. Technol. 74 (2013) 221–227, doi:10.1016/j.compscitech.2012.11.015.
[25] S. Araby, N. Saber, X. Ma, N. Kawashima, H. Kang, H. Shen, L. Zhang, J. Xu, P. Majewski, J. Ma, Implication of multi-walled carbon nanotubes on polymer/graphene composites, Mater. Des. 65 (2015) 690–699, doi:10.1016/j.matdes.2014.09.069.
[26] H. Im, J. Kim, Thermal conductivity of a graphene oxide-carbon nanotube hybrid/epoxy composite, Carbon N. Y. 50 (2012) 5429–5440, doi:10.1016/j.carbon.2012.07.029.
[27] J. López-Barroso, A.L. Martínez-Hernández, J.L. Rivera-Armenta, C. Velasco-Santos, Multidimensional nanocomposites of epoxy reinforced with 1D and 2D carbon nanostructures for improve fracture resistance, Polymers (Basel) 10 (2018) 281–296, doi:10.3390/polym10030281.
[28] E. Jimenez-Cervantes Amieva, J. López-Barroso, A.L. Martínez-Hernández, C. Velasco-Santos, Graphene-based materials functionalization with natural polymeric biomolecules, in: PK Nayak (Ed.), Recent Advances in Graphene Research, InTech, 2016, pp. 257–298.
[29] N. Domun, H. Hadavinia, T. Zhang, T. Sainsbury, G.H. Liaghat, S. Vahid, Improving the fracture toughness and the strength of epoxy using nanomaterials-a review of the current status, Nanoscale 7 (2015) 0294–10329, doi:10.1039/c5nr01354b.
[30] X. Yan, J. Gu, G. Zheng, J. Guo, A.M. Galaska, J. Yu, M.A. Khan, L. Sun, D.P. Young, Q. Zhang, S. Wei, Z. Guo, Lowly loaded carbon nanotubes induced high electrical conductivity and giant magnetoresistance in ethylene/1-octene copolymers, Polymer (Guildf) 103 (2016) 315–327, doi:10.1016/j.polymer.2016.09.056.
[31] J.-X. Zhang, Y.-X. Liang, X. Wang, H.-J. Zhou, S.-Y. Li, J. Zhang, Y. Feng, N. Lu, Q. Wang, Z. Guo, Strengthened epoxy resin with hyperbranched polyamine-ester anchored graphene oxide via novel phase transfer approach, Adv. Compos. Hybrid Mater. 1 (2018) 300–309, doi:10.1007/s42114-017-0007-0.
[32] M. Abdalla, D. Dean, D. Adibempe, E. Nyairo, P. Robinson, G. Thompson, The effect of interfacial chemistry on molecular mobility and morphology of multiwalled carbon nanotubes epoxy nanocomposite, Polymer (Guildf) 48 (2007) 5662–5670, doi:10.1016/j.polymer.2007.06.073.
[33] L.W. Hill, Calculation of crosslink density in short chain networks, Prog. Org. Coat. 31 (1997) 235–243, doi:10.1016/S0300-9440(97)00081-7.
[34] J.S. Nakka, K.M.B. Jansen, L.J. Ernst, Effect of chain flexibility in the network structure on the viscoelasticity of epoxy thermosets, J. Polym. Res. 18 (2011) 1879–1888, doi:10.1007/s10965-011-9595-5.
[35] B. Ramezanzadeh, M.M. Attar, M. Farzam, Effect of ZnO nanoparticles on the thermal and mechanical properties of epoxy-based nanocomposite, J. Therm. Anal. Calorim. 103 (2011) 731–739, doi:10.1007/s10973-010-0996-1.
[36] M.R. Gude, S.G. Prolongo, A. Ureña, Effect of the epoxy/amine stoichiometry on the properties of carbon nanotube/epoxy composites, J. Therm. Anal. Calorim. 108 (2012) 717–723, doi:10.1007/s10973-011-2056-x.
[37] A.H. Farhadian, M.K. Tehrani, M.H. Keshavarz, S.M.R. Darbani, Raman spectroscopy combined with principle component analysis to investigate the aging of high energy materials, Laser Phys. 27 (2017) 075701–075708, doi:10.1088/1555-6611/AA7485.
[38] M.W. Smith, I. Dallmeyer, T.J. Johnson, C.S. Brauer, J.- S. McEwen, J.F. Espinal, M. Garcia-Perez, Structural analysis of char by Raman spectroscopy: improving band assignments through computational calculations from first principles, Carbon N Y 100 (2016) 678–692, doi:10.1016/j.carbon.2016.01.031.
[39] T. Visser, J.H. Van Der Maas, Systematic interpretation of Raman spectra of organic compounds. II-Ethers, J. Raman Spectrosc. 6 (1977) 114–116, doi:10.1002/jrs.1250060303.

[40] J.M. Chalmers, R.W. Hannah, D.W. Mayo, Spectra–structure correlations: polymer spectra, in: P. Griffiths, J.M. Chalmers (Eds.), Handbook of Vibrational Spectroscopy, Wiley, Chichester (UK), 2006, pp. 1–26.
[41] R.A. Nyquist, Interpreting infrared, Raman, and nuclear magnetic resonance spectra, in: Chapter 9, Benzene and Its Derivatives, Elsevier Academic Press, 2001, pp. 351–423.
[42] Y. Furukawa, F. Ueda, Y. Hyodo, I. Harada, T. Nakajima, T. Kawagoe, Vibrational spectra and structure of polyaniline, Macromolecules 21 (1988) 1297–1305, doi:10.1021/ma00183a020.
[43] C. Castiglioni, Theory of vibrational spectroscopy of polymers, in: P. Griffiths, J.M. Chalmers (Eds.), Handbook of Vibrational Spectroscopy, Wiley, Chichester (UK), 2007, pp. 1–31, doi:10.1002/9780470027325.s8916.
[44] M.S. Dresselhaus, A. Jorio, R. Saito, Characterizing graphene, graphite, and carbon nanotubes by Raman spectroscopy, Annu. Rev. Condens. Matter Phys. 1 (2010) 89–108, doi:10.1146/annurev-conmatphys-070909-103919.
[45] S. Michielsen, Application of Raman spectroscopy to organic fibers and films, in: R.I. Lewis, H.G.M. Edwards (Eds.), Handbook of Raman Spectroscopy, From the Research Laboratory to the Process Line, CRC Press, Boca Raton, 2001, pp. 749–799.
[46] K. Papagelis, Raman spectroscopy of carbon nanotube–polymer hybrid materials, in: D. Tasis (Ed.), Carbon Nanotube-Polymer Composites, Royal Society of Chemistry, 2013, pp. 253–269, doi:10.1039/9781849736817-00253.
[47] S. Laurenzi, S. Botti, A. Rufoloni, M. G. Santonicola, Fracture mechanisms in epoxy composites reinforced with carbon nanotubes, Proc. Eng. (2014) 157–164 2014 Sep 14-17, doi:10.1016/j.proeng.2014.11.139.
[48] A.S. Paipetis, Stress induced changes in the Raman spectrum of carbon nanostructures and their composites, in: A. Paipetis, V. Kostopoulos (Eds.), Carbon Nanotube Enhanced Aerospace Composite materials. Solid mechanics and Its Applications, Springer, Dordrecht, Netherlands, 2013, pp. 185–217.
[49] X. Wang, J. Wang, W. Zhao, L. Zhang, X. Zhong, R. Li, J. Ma, Synthesis and characterization of thermotropic liquid crystalline polyester/multi-walled carbon nanotube nanocomposites, Appl. Surf. Sci. 256 (2010) 1739–1743, doi:10.1016/j.apsusc.2009.09.105.
[50] M. Tedesco, M.C. Chain, E.A. Bortoluzzi, L. da F.R. Garcia, A.M.H. Alves, C.S. Teixeira, Comparison of two observational methods, scanning electron and confocal laser scanning microscopies, in the adhesive interface analysis of endodontic sealers to root dentine, Clin. Oral Invest. 22 (2018) 2353–2361, doi:10.1007/s00784-018-2336-y.
[51] M. Marchena, D. Janner, T.L. Chen, V. Finazzi, V. Pruneri, Low temperature direct growth of graphene patterns on flexible glass substrates catalysed by a sacrificial ultrathin Ni film, Opt. Mater. Express 6 (2016) 2487–2507, doi:10.1364/ome.6.002487.
[52] M. Roman, K.M. Marzec, E. Grzebelus, P.W. Simon, M. Baranska, R. Baranski, Composition and (in)homogeneity of carotenoid crystals in carrot cells revealed by high resolution Raman imaging, Spectrochim. Acta A Mol. Biomol. Spectrosc. 136 (2015) 1395–1400 136, doi:10.1016/j.saa.2014.10.026.
[53] S.Y. Yang, W.N. Lin, Y.L. Huang, H.-W. Tien, J.-Y. Wang, C.C.M. Ma, S.-M. Li, Y.-S. Wang, Synergetic effects of graphene platelets and carbon nanotubes on the mechanical and thermal properties of epoxy composites, Carbon N. Y. 49 (2011) 793–803, doi:10.1016/j.carbon.2010.10.014.
[54] S. Chatterjee, F. Nafezarefi, N.H. Tai, L. Schlagenhauf, F.A. Nüesch, B.T.t. Chu, Size and synergy effects of nanofiller hybrids including graphene nanoplatelets and carbon nanotubes in mechanical properties of epoxy composites, Carbon N. Y. 50 (2012) 5380–5386, doi:10.1016/j.carbon.2012.07.021.
[55] M. Safdari, M.S. Al-Haik, Synergistic electrical and thermal transport properties of hybrid polymeric nanocomposites based on carbon nanotubes and graphite nanoplatelets, Carbon N. Y. 64 (2013) 111–121, doi:10.1016/j.carbon.2013.07.042.
[56] E. Dervishi, F. Hategekimana, L. Boyer, F. Watanabe, T. Mustafa, A. Biswas, A.R. Biris, A.S. Biris, The effect of carbon nanotubes and graphene on the mechanical properties of multi-component polymeric composites, Chem. Phys. Lett. 590 (2013) 126–130, doi:10.1016/j.cplett.2013.10.060.
[57] L. Yue, G. Pircheraghi, S.A. Monemian, I. Manas-Zloczower, Epoxy composites with carbon nanotubes and graphene nanoplatelets - Dispersion and synergy effects, Carbon N. Y. 78 (2014) 268–278, doi:10.1016/j.carbon.2014.07.003.
[58] X.-J. Shen, X.-Q. Pei, Y. Liu, S.-Y. Fu, Tribological performance of carbon nanotube–graphene oxide hybrid/epoxy composites, Compos. Part B Eng. 57 (2014) 120–125, doi:10.1016/J.COMPOSITESB.2013.09.050.
[59] M.K. Shukla, K. Sharma, Improvement in mechanical and thermal properties of epoxy hybrid composites by functionalized graphene and carbon-nanotubes, Mater. Res. Express 6 (2019) 085318–085331, doi:10.1088/2053-1591/ab1cc2.
[60] Y.M. Jen, J.C. Huang, Synergistic effect on the thermomechanical and electrical properties of epoxy composites with the enhancement of carbon nanotubes and graphene nanoplatelets, Materials (Basel) 12 (2019) 255–266, doi:10.3390/ma12020255.
[61] Y. Li, R. Umer, A. Isakovic, Y.A. Samad, L. Zheng, Y.K. Liao, Synergistic toughening of epoxy with carbon nanotubes and graphene oxide for improved long-term performance, RSC Adv. 3 (2013) 8849–8856, doi:10.1039/C3RA22300K.
[62] X. Li, J. Wang, One-dimensional and two-dimensional synergized nanostructures for high-performing energy and conversion, InfoMat 2 (2020) 3–32, doi:10.1002/inf2.12040.
[63] J. Wang, X. Jin, H. Wu, S. Guo, Polyimide reinforced with hybrid graphene oxide @ carbon nanotube: toward high strength, toughness, electrical conductivity, Carbon N. Y. 123 (2017) 502–513, doi:10.1016/j.carbon.2017.07.055.
[64] N. Yousefi, X. Lin, Q. Zheng, X. Shen, J.R. Pothnis, J. Jia, J. Ja, E. Zussman, J.-K. Kim, Simultaneous in situ reduction, self-alignment and covalent bonding in graphene oxide/epoxy composites, Carbon N. Y. 59 (2013) 406–417, doi:10.1016/j.carbon.2013.03.034.
[65] A. Montazeri, K. Pourshamsian, M. Riazian, Viscoelastic properties and determination of free volume fraction of multi-walled carbon nanotube/epoxy composite using dynamic mechanical thermal analysis, Mater. Des. 36 (2012) 408–414, doi:10.1016/j.matdes.2011.11.038.
[66] Z. Zhao, Q. Zhang, D. Chen, P. Lu, Enhanced mechanical properties of graphene-based poly(vinyl alcohol) composites, Macromolecules 43 (2010) 2357–2363, doi:10.1021/ma902862u.
[67] G. Gkikas, N.M. Barkoula, A.S. Paipetis, Effect of dispersion conditions on the thermo-mechanical and toughness properties of multi walled carbon nanotubes-reinforced epoxy, Compos. B Eng. 43 (2012) 2697–2705, doi:10.1016/j.compositesb.2012.01.070.
[68] H. Gu, S. Tadakamalla, X. Zhang, X. Zhang, Y. Huang, Y. Jiang, H.A. Colorado, Z. Luo, S. Wei, Z. Guo, Epoxy resin nanosuspensions and reinforced nanocomposites from polyaniline stabilized multi-walled carbon nanotubes, J. Mater. Chem. C 1 (2013) 729–743, doi:10.1039/c2tc00379a.
[69] T. K. Bindu Sharmila, A.B. Nair, B.T. Abraham, B.T. A.braham, P.M. Sabura Begum, E.T. Thachil, Microwave exfoliated reduced graphene oxide epoxy nanocomposites for high performance applications, Polymer (Guildf) 55 (2014) 3614–3627, doi:10.1016/j.polymer.2014.05.032.
[70] C. Monteserín, M. Blanco, E. Aranzabe, A. Aranzabe, J.M. Laza, A. Larrañaga-Varga, J.L. Vilas, Effects of graphene oxide and chemically-reduced graphene oxide on the dynamic mechanical properties of epoxy amine composites, Polymers (Basel) 9 (2017) 449, doi:10.3390/polym9090449.
[71] L.S. Cividanes, E.A.N. Simonetti, M.B. Moraes, F.W. Fernandes, G.P. Thim, Influence of carbon nanotubes on epoxy resin cure reaction using different techniques: a comprehensive review, Polym. Eng. Sci. 54 (2014) 2461–2469, doi:10.1002/pen.23775.
[72] R.P. Chartoff, J.D. Menczel, S.H. Dillman, Dynamic Mechanical Analysis (DMA), in: JD Menczel, RB Prime (Eds.), Thermal Analysis of Polymers: Fundamentals and Applications, Wiley, Hoboken (NJ), 2008, pp. 387–495, doi:10.1002/9780470423837.ch5.
[73] D.G.D. Galpaya, J.F.S. Fernando, L. Rintoul, N. Motta, E.R. Waclawik, C. Yang, G.A. George, The effect of graphene oxide and its oxidized debris on the cure chemistry and interphase structure of epoxy nanocomposites, Polymer (Guildf) 71 (2015) 122–134, doi:10.1016/j.polymer.2015.06.054.
[74] O. Starkova, S. Chandrasekaran, L.A.S.A. Prado, F. Tölle, M.K. Schulte, Hydrothermally resistant thermally reduced graphene oxide and multi-wall carbon nanotube based epoxy nanocomposites, Polym. Degrad. Stab. 998 (2013) 519–526, doi:10.1016/j.polymdegradstab.2012.12.005.
[75] H. Gu, C. Ma, J. Gu, J. Guo, X. Yan, J. Huang, Q. Zhang, Z. Guo, An overview of multifunctional epoxy nanocomposites, J. Mater. Chem. C 4 (2016) 5890–5906, doi:10.1039/C6TC01210H.
[76] P.C. Ma, N.A. Siddiqui, G. Marom, J.-K. Kim, Dispersion and functionalization of carbon nanotubes for polymer-based nanocomposites: a review, Compos. Part A Appl. Sci. 41 (2010) 1345–1367, doi:10.1016/j.compositesa.2010.07.003.
[77] L.C. Tang, Y.J. Wan, D. Yan, Y.-B. Pen, L. Zhao, Y.-B. Li, L.-B. Wu, J.-X. Jiang, G.-Q. Lai, The effect of graphene dispersion on the mechanical properties of graphene/epoxy composites, Carbon N. Y. 60 (2013) 16–27, doi:10.1016/j.carbon.2013.03.050.
[78] J. Wei, M.S. Saharudin, T. Vo, F. Inam, Dichlorobenzene: an effective solvent for epoxy/graphene nanocomposites preparation, R. Soc. Open Sci. 4 (2017) 170778–1707787, doi:10.1098/rsos.170778.
[79] J. Jia, X. Sun, X. Lin, X. Shen, Y.-W. Mai, J.-K. Kim, Exceptional electrical conductivity and fracture resistance of 3D interconnected graphene foam/epoxy composites, ACS Nano 8 (2014) 5774–5783, doi:10.1021/nn500590g.
[80] Q.P. Feng, J.P. Yang, S.Y. Fun, Y.-W. Mai, Synthesis of carbon nanotube/epoxy composite films with a high nanotube loading by a mixed-curing-agent assisted layer-by-layer method and their electrical conductivity, Carbon N. Y. 48 (2010) 2057–2062, doi:10.1016/j.carbon.2010.02.016.
[81] N.P. Singh, V.K. Gupta, A.P. Singh, Graphene and carbon nanotube reinforced epoxy nanocomposites: a review, Polymer (Guildf) 180 (2019) 121724, doi:10.1016/j.polymer.2019.121724.
[82] S. Chandrasekaran, N. Sato, F. Tölle, R. Mülhaupt, B. Fiedler, K. Schulte, Fracture toughness and failure mechanism of graphene based epoxy composites, Compos. Sci. Technol. 97 (2014) 90–99, doi:10.1016/j.compscitech.2014.03.014.
[83] G. Gkikas, A.S. Paipetis, Optimisation and analysis of the reinforcement effect of carbon nanotubes in a typical matrix system, Meccanica 50 (2015) 461–478, doi:10.1007/s11012-014-9915-z.
[84] I. Charitos, G. Georgousis, P.A. Klonos, A. Kyritsis, D. Mouzakis, Y. Raptis, A. Kontos, E. Kontou, The synergistic effect on the thermomechanical and electrical properties of carbonaceous hybrid polymer nanocomposites, Polym. Test 95 (2021) 1071102, doi:10.1016/j.polymertesting.2021.107102.